ChemComm

COMMUNICATION

View Article Online
View Journal | View Issue

Cite this: *Chem. Commun.*, 2021, **57**, 8937

Received 10th July 2021,
Accepted 9th August 2021

DOI: 10.1039/d1cc03431f

rsc.li/chemcomm

A well-defined dual Mn-site based metal–organic framework to promote CO_2 reduction/evolution in Li–CO_2 batteries†

Long-Zhang Dong, ‡[a] Yu Zhang, ‡[a] Yun-Feng Lu,[a] Lei Zhang,[a] Xin Huang,[a] Jian-Hui Wang,[a] Jiang Liu,[a] Shun-Li Li*[a] and Ya-Qian Lan *[ab]

A series of Li–CO_2 battery cathode materials are reported based on metal–organic frameworks with dual-metal sites containing a metalloporphyrin and a metal-coordinated pyrazole. MnTPzP-Mn demonstrates a low voltage hysteresis of 1.05 V at 100 mA g^{-1} and good stability of 90 cycles at 200 mA g^{-1}. Among them, the Mn-coordinated pyrazole site can promote the effective decomposition of Li_2CO_3, and the Mn-metalloporphyrin site contributes to the activation of CO_2. This is the first example of using a crystalline cathode material with a well-defined structure to reveal natural catalytic sites for CO_2 reduction/evolution reactions under aprotic conditions in Li–CO_2 batteries.

Due to the increasingly severe greenhouse effect and energy crisis, many countries plan to achieve carbon neutrality.[1] Therefore, a considerable number of researchers have turned their attention to recycling CO_2 and the development of clean energy.[2] As a new type of energy storage device, the Li–CO_2 battery not only provides an effective form of CO_2 recycling but also has a high energy density of 1876 W h kg^{-1}, much higher than that of the lithium-ion battery of 265 W h kg^{-1}, and thus attracts widespread attention from researchers around the world.[3] However, considering that the CO_2 molecule is chemically inert, and the discharge product (usually Li_2CO_3) is a wide bandgap insoluble insulator, it causes sluggish kinetics of the CO_2 reduction reaction and difficultly decomposing the Li_2CO_3.[4] Furthermore, based on the above mentioned findings, Li–CO_2 batteries have problems such as low energy conversion efficiency, slow charging and discharging rates, and short cycle life, which essentially limits the practical application of Li–CO_2 batteries.[3b,5]

The development of efficient Li–CO_2 battery electrode materials is the key to improving their performance in terms of capacity, working potential, and cycling stability.[3a,5a] However, the two main challenges of constructing high-performance Li–CO_2 battery electrodes are as follows: first, the electrochemical inertness of Li_2CO_3 makes it hard to decompose into CO_2 efficiently and effectively;[6] secondly, the chemically inert CO_2 catalytic reduction kinetics are slow under aprotic conditions.[7] So far, researchers have explored a variety of materials that can work as a cathode for Li–CO_2 batteries, including various carbon materials,[7a,8] transition metal oxides,[9] and precious metal nanoparticles.[10] Recently, researchers have reported that electrode materials containing Ir[10a] or Ru[10c–e] nanoparticles have a significant effect on boosting the decomposition of Li_2CO_3, promoting the reaction kinetics, and reducing the overpotential during charging. Besides, except for expensive precious metals, transition metal manganese-based materials have also been reported to promote the decomposition of Li_2CO_3.[9c,d,11] For example, Wang *et al.*[9c] reported that the MnO/graphene composite could enable 0.88 V voltage hysteresis at 50 mA g^{-1}. In addition, other Mn-based oxides (*e.g.*, Mn_2O_3,[9d] Mn_3O_4[12]) have also been reported to exhibit improved electrochemical performance. Indeed, there have been a lot of research works to develop effective Li–CO_2 battery electrode materials, and significant progress has been made to date, but there is still a lack of electrode materials with precise structures for exploring their complex mechanisms.

Metal–organic frameworks (MOFs), as a class of crystalline materials with porous, well-defined, highly adjustable structures and an open-metal site, are promising candidates for Li–CO_2 battery electrode materials.[13] Wang *et al.*[11a] found that the open Mn-site in a MOF (Mn_2dobdc) is the catalytically active site for Li_2CO_3 decomposition with a low charge potential

[a] *Jiangsu Collaborative Innovation Centre of Biomedical Functional Materials, Jiangsu Key Laboratory of New Power Batteries, School of Chemistry and Materials Science, Nanjing Normal University, Nanjing 210023, P. R. China. E-mail: slli@njnu.edu.cn, yqlan@m.scnu.edu.cn, yqlan@njnu.edu.cn Web: http://www.yqlangroup.com*

[b] *School of Chemistry, South China Normal University, Guangzhou, 510006 P. R. China*

† Electronic supplementary information (ESI) available. CCDC 2087766–2087768. For ESI and crystallographic data in CIF or other electronic format see DOI: 10.1039/d1cc03431f

‡ These authors contributed equally to the manuscript.

plateau of ~3.96 V at 50 mA g^{-1}. In addition, Mn-TTCOF[11b] has a discharged potential plateau of 2.92 V, revealing that Mn-metalloporphyrin is the active site for catalyzing CO_2 reduction. Through the above-mentioned research, Li–CO_2 battery electrode materials should have the following features: (1) Li-ion transfer pathways, (2) CO_2 adsorption capacity, and (3) catalyzing the CO_2 reduction/evolution reaction.

Therefore, we designed and synthesized three porphyrin-based 2-dimensional MOFs **MTPzP-M** (**MnTPzP-Mn**, **CoTPzP-Mn**, **CoTPzP-Co**) through self-assembly of the 5,10,15,20-tetra(1*H*-pyrazol-4-yl)porphyrin[14] (TPzP) ligand and transition metal Mn or Co ions. There are two metal sites in these three compounds, of which one is the metal site of the metalloporphyrin (M-Por, M = Mn, Co), and the other is coordinated with four pyrazole groups of the TPzP ligands (M-Pz). We expect that between the double Mn-site within **MnTPzP-Mn**, Mn-Pz can promote the complete and effective decomposition of Li_2CO_3, and the Mn-Por may contribute to the activation of CO_2. The results of Li–CO_2 battery tests display that **MnTPzP-Mn** as an electrode material shows a low terminal potential gap of 1.05 V between charge and discharge at 100 mA g^{-1}. Furthermore, the battery can be cycled well up to 90 cycles at 200 mA g^{-1}. The combination of the dual Mn-sites can achieve effective CO_2 reduction and Li_2CO_3 decomposition. We designed a series of crystalline electrode materials with well-defined crystal structures to reveal the catalytically active sites in the aprotic Li–CO_2 battery system.

MTPzP-M (M = Co, Mn) are synthesized using the solvothermal method with Mn or Co sulfate and TPzP or TPzP-Mn ligand in *N*,*N*-dimethylformamide. The single-crystal X-ray diffraction (SC-XRD) experiments proved that a series of three crystals (**MnTPzP-Mn**, **CoTPzP-Mn**, **CoTPzP-Co**) crystallize in the same orthorhombic space group *Pmna* (Tables S1–S3, ESI†). In addition, the structures solved by the SC-XRD experiments show that these crystals are almost isomorphic. The asymmetric units of their structures all contain a half Mn or Co ion, one sulfate radical, a half TPzP-Mn or TPzP-Co, a half dimethylamine cation, and a half Cl^- or H_2O (Fig. S1, ESI†). Take **MnTPzP-Mn** as an example: the coordination environment of TPzP is that each pyrazolyl group coordinated with Mn1 and the porphyrin ring coordinates with Mn2; Mn1 coordinates with four Pz groups from four TPzP ligands and two sulfate radicals as a 4-c node (Fig. S2, ESI†). The above coordination mode constructed a 4,4-c net sql topology 2D framework (Fig. 1a), and thus through π–π interaction and hydrogen bonding formed a 3D stacked structure, as shown in Fig. 1a and Fig. S3 (ESI†). The solvent surface of **MnTPzP-Mn** is shown in Fig. 1b, and the free volume is calculated to be 26.9% by PLATON[15] software. The PXRD spectra of the samples synthesized are consistent with the simulated spectra, indicating that they all have good crystallinity and purity (Fig. 1c). At the same time, the PXRD spectra of the samples soaked in the electrolyte for 72 hours are also consistent, proving that they have good chemical stability under a battery test environment (Fig. S4, ESI†). Simultaneously, the Fourier transform infrared spectroscopy (FTIR) pattern is performed to disclose the structural characteristic

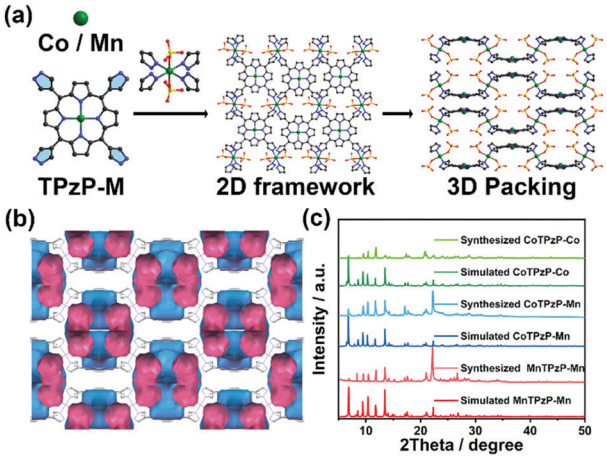

Fig. 1 (a) 2D framework of **MTPzP-M** constructed by the Co or Mn sulfate and TPzP-M (M = Co, Mn) and 3D packing mode. (b) The solvent surface of **MnTPzP-Mn**. (c) PXRD patterns of **MTPzP-M**.

of **MTPzP-M** (Fig. S5, ESI†). And the thermogravimetric analysis (TGA) indicates that **MTPzP-M** has good thermal stability of *ca.* 300 °C (Fig. S6, ESI†).

The Li–CO_2 battery performances of the synthesized **MTPzP-M** MOFs with different dual metal sites have been evaluated to illustrate the impact of both metal sites on the battery reactions.

The discharge/charge curves of different cathodes cycled at a current density of 100 mA g^{-1} with a limited capacity of 1000 mA h g^{-1} were recorded first. As shown in Fig. 2a, **CoTPzP-Co** exhibits the worst performance among the three samples with a high charge potential of 4.56 V and a low potential of 2.65 V. In comparison, both **MnTPzP-Mn** and **CoTPzP-Mn** show similar discharge potential plateaus at the first cycle with relatively

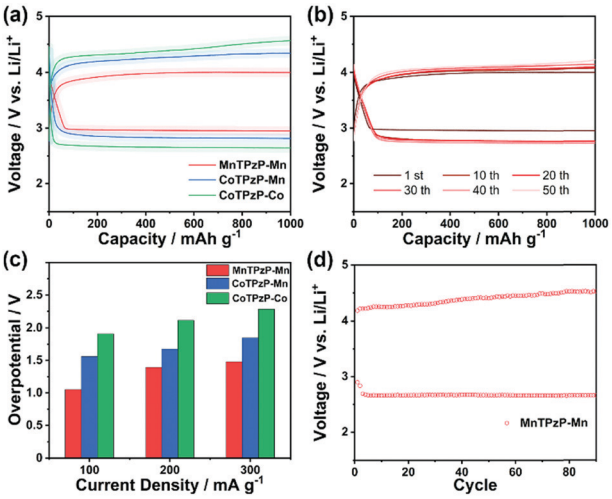

Fig. 2 (a) The first cycle charge/discharge curve of **MTPzP-M** cathodes with a limited capacity of 1000 mA h g^{-1} at 100 mA g^{-1}. (b) Charge/discharge cycling curves of **MnTPzP-Mn** with the limited capacity of 1000 mA h g^{-1} at 100 mA g^{-1}. (c) The overpotentials of **MTPzP-M** cathodes under current densities of 100 mA g^{-1}, 200 mA g^{-1}, and 300 mA g^{-1}. (d) Long-term cycling of the **MnTPzP-Mn** cathode at the current density of 200 mA g^{-1}.

high terminal potentials of 2.95 V and 2.82 V, respectively. This implies that the presence of the Mn-Por site in **MTPzP-Mn** MOFs is beneficial to the aprotic CO_2 reduction during the discharge process, which is consistent with the previous research.[9c,11a] However, the charge potential of **CoTPzP-Mn** (4.56 V) is much higher than that of **MnTPzP-Mn** (4.00 V), suggesting that it is Mn-Pz rather than Co-Pz that works for Li_2CO_3 decomposition during the charging process. Furthermore, the cyclic voltammogram (CV) curve under CO_2 shows more obvious redox peaks and higher polarization current than the one tested under Ar, demonstrating the CO_2 reduction and evolution reaction activity on the **MnTPzP-Mn** cathode (Fig. S7, ESI†). Additionally, the cycling tests at 100 mA g^{-1} are presented in Fig. 2b, Fig. S8 and S9 (ESI†), in which **MnTPzP-Mn** shows discharge and charge potential plateaus of 2.72 V and 4.22 V after 50 cycles. On the contrary, the **CoTPzP-Co** cathode even discharged down to 2.43 V at the 20th cycle, indicating intensified battery polarization (Fig. S9, ESI†). Preliminarily, according to these battery test results, it could be speculated that Mn-Por and Mn-Pz sites may play positive roles in activating CO_2 reduction and Li_2CO_3, respectively.

The Li–CO_2 battery performances of **MTPzP-M** MOFs at different current densities have also been assessed (Fig. S10–S12, ESI†). The **MnTPzP-Mn** cathode shows high discharge potentials ($>$ 2.80 V) and low charge potentials ($<$ 4.32 V) at all current densities, which mainly originates from the catalytic activity of the dual Mn-sites. The calculated overpotentials, the voltage gaps between the terminal discharge potentials and charge potentials, are summarized in Fig. 2c. Impressively, the overpotential of the first cycle on the **MnTPzP-Mn** cathode is only $\sim$1.05 V, which is comparable to the best Li–CO_2 battery cathode catalysts so far (Table S4, ESI†). And it also shows low overpotentials of 1.39 V and 1.48 V at 200 mA g^{-1} and 300 mA g^{-1}, respectively. In comparison, **CoTPzP-Co** hardly exhibits Li–CO_2 battery activity at all current densities, and the charge terminal potential even reaches up to 4.76 V at a large current density of 300 mA g^{-1}. The long-term cycling of **MnTPzP-Mn** was further carried out at 200 mA g^{-1}. As shown in Fig. 2d, the battery is able to continuously work for 90 cycles with a stable discharge potential, exhibiting excellent cycling performance.

The full discharge/charge curves obtained at 100 mA g^{-1} from 2.0 to 4.5 V *vs.* Li/Li^+ are presented to investigate the reversibility of the synthesized MOF cathodes. As shown in Fig. 3a, **MnTPzP-Mn** and **CoTPzP-Mn** reached full discharge capacities of 14 025 mA h g^{-1} and 12 884 mA h g^{-1}, respectively, much higher than that of **CoTPzP-Co** (8456 mA h g^{-1}). In addition, it also demonstrates that only the **MnTPzP-Mn** assembled battery is reversible and could be fully recharged back after the deep discharge process, which further verifies that the Mn-Pz site plays a key role in activating the charge reaction. Moreover, the electrochemical impedance spectroscopy (EIS) also proves the reversibility of the **MnTPzP-Mn** based Li–CO_2 battery. As shown in Fig. S13 (ESI†), the cell impedance substantially increased, accompanied by discharge proceeding due to the generation of insulated discharge products. And when the cell recharged back, the EIS plots show

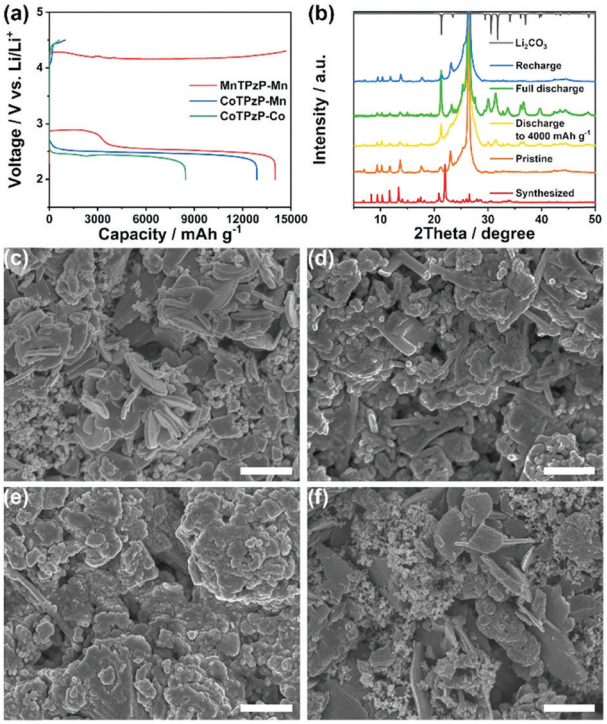

Fig. 3 (a) The full discharge/charge curves of **MTPzP-M** MOF cathodes recorded within 2.0–4.5 V *vs.* Li/Li^+. (b) The XRD patterns of **MnTPzP-Mn** cathodes at different discharge or charge stages and the PDF card of Li_2CO_3. SEM images of **MnTPzP-Mn** cathodes at different discharge or charge stages, scale bar: 2 μm. (c) pristine, (d) discharge to 4000 mA h g^{-1}, (e) full discharge to 2.0 V *vs.* Li/Li^+, and (f) recharge back from (e).

similar interfacial, charge transfer, and ion diffusion resistances to the pristine one, suggesting that most of the generated discharge products were decomposed upon being charged. In addition, the discharge products on **MTPzP-M** MOF cathodes are all crystalline Li_2CO_3 (PDF# 22-1141), according to the XRD patterns shown in Fig. 3b and Fig. S14 and S15 (ESI†). For all the three cathode materials, the diffraction peaks intensity of Li_2CO_3 increased with the discharge capacity rising from 4000 mA h g^{-1} to the full discharge state. However, only the **MnTPzP-Mn** cathode no longer exhibited Li_2CO_3 peaks after recharge, indicating that the Mn-Pz site is essential to the decomposition of Li_2CO_3 upon charge. The scanning electron microscope (SEM) images of the corresponding electrodes with different states were taken to observe the morphology change on the cathode surface. As shown in Fig. 3c–f, plate-like **MnTPzP-Mn** surrounded by small KB particles could be seen on the pristine cathode. And **MnTPzP-Mn** was coated with Li_2CO_3 particles when discharged to 4000 mA h g^{-1} and even covered up when the cell was fully discharged. **MnTPzP-Mn** with a plate-like shape appeared again after recharge and the cathode surface was loose without obvious Li_2CO_3 particles. On the contrary, according to the SEM images shown in Fig. S14c and S15c (ESI†), the **CoTPzP-Mn** and **CoTPzP-Co** cathode surfaces were dense after recharge and small Li_2CO_3 particles were covered on the cathode catalysts, indicating incomplete decomposition of Li_2CO_3.

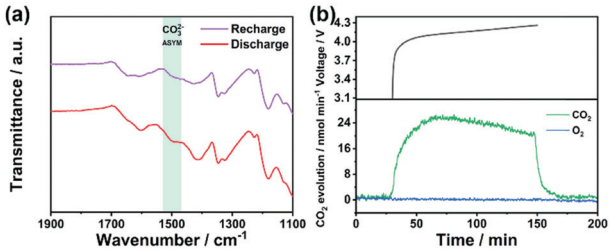

Fig. 4 (a) ATR-FIIR spectra of the discharged and recharged **MnTPzP-Mn** cathode. (b) *In situ* DEMS during charging over the **MnTPzP-Mn** based Li–CO_2 battery.

Based on the attenuated total reflection Fourier transform infrared (ATR-FTIR) spectra collected from the cathode at discharged and recharged stages during cycling, the asymmetrical stretching vibration of CO_3^{2-} in Li_2CO_3 significantly weakened, indicating almost complete decomposition of Li_2CO_3. In order to further study the charge reaction products of the proposed **MnTPzP-Mn** based Li–CO_2 system, an *in situ* differential electrochemical mass spectrometry (DEMS) test was carried out to monitor the generated gas products during the charging process. It can be observed from Fig. 4b that a CO_2 signal appears during the charging process, and there is almost no change in the O_2 signal, suggesting that only CO_2 is generated during the charging reaction. In addition, according to the CO_2 yield and capacity of charge in the DEMS test, the calculated charge-to-mass ratio over the **MnTPzP-Mn** based Li–CO_2 system is determined to be $4.04e^-/3CO_2$. Therefore, combined with the results of XRD, *in situ* DEMS, and the battery performance evaluation, it could be inferred that the reversible discharge/charge reaction on the **MnTPzP-Mn** cathode should be $4Li^+ + 3CO_2 + 4e^- \rightarrow 2Li_2CO_3 + C$ (E^0 = 2.80 V *vs.* Li/Li^+).[16]

In summary, we designed a series of dual-metal-site MOF-based (**MTPzP-M**) Li–CO_2 battery cathode catalysts. Herein, the **MnTPzP-Mn** cathode exhibits the lowest voltage hysteresis of 1.05 V and excellent stability of 90 cycles at 200 mA g^{-1}, which is comparable to the current state-of-the-art Li–CO_2 battery cathode materials. The Li–CO_2 battery performance evaluation together with the characterizations including XRD, SEM and ATR-FTIR tests suggest that the dual Mn-sites of the Mn-Por site and Mn-Pz site in the **MnTPzP-Mn** cathode catalyst are the intrinsic active sites for promoting aprotic CO_2 reduction reaction during discharging and facilitating the complete decomposition of Li_2CO_3 during charging, respectively. In addition, the *in situ* DEMS test was employed to investigate the battery reaction mechanism of the **MnTPzP-Mn** cathode by monitoring CO_2 evolution and charge capacity. The crystalline cathode materials we designed with well-defined crystal structures provide new insights for revealing the catalytically active sites in the aprotic Li–CO_2 battery system.

This work was financially supported by NSFC (No. 21871141, 21871142, 22071109 and 92061101); Priority Academic Program Development of Jiangsu Higher Education Institutions and the Foundation of Jiangsu Collaborative Innovation Center of Biomedical Functional Materials.

Conflicts of interest

There are no conflicts to declare.

Notes and references

1 H. L. van Soest, M. G. J. den Elzen and D. P. van Vuuren, *Nat. Commun.*, 2021, **12**, 2140.
2 (*a*) J. Xie, Z. Zhou and Y. Wang, *Adv. Funct. Mater.*, 2020, **30**, 1908285; (*b*) Y. Y. Birdja, E. Pérez-Gallent, M. C. Figueiredo, A. J. Göttle, F. Calle-Vallejo and M. T. M. Koper, *Nat. Energy*, 2019, **4**, 732–745; (*c*) D. Schimel, B. B. Stephens and J. B. Fisher, *Proc. Natl. Acad. Sci. U. S. A.*, 2015, **112**, 436.
3 (*a*) X. Mu, H. Pan, P. He and H. Zhou, *Adv. Mater.*, 2020, **32**, 1903790; (*b*) Z. Xie, X. Zhang, Z. Zhang and Z. Zhou, *Adv. Mater.*, 2017, **29**, 1605891.
4 (*a*) C. Yang, K. Guo, D. Yuan, J. Cheng and B. Wang, *J. Am. Chem. Soc.*, 2020, **142**, 6983–6990; (*b*) Z. Zhang, W.-L. Bai, K.-X. Wang and J.-S. Chen, *Energy Environ. Sci.*, 2020, **13**, 4717–4737.
5 (*a*) Y. Qiao, J. Yi, S. Wu, Y. Liu, S. Yang, P. He and H. Zhou, *Joule*, 2017, **1**, 359–370; (*b*) A. Hu, C. Shu, C. Xu, R. Liang, J. Li, R. Zheng, M. Li and J. Long, *J. Mater. Chem. A*, 2019, **7**, 21605–21633.
6 (*a*) B. Liu, Y. Sun, L. Liu, J. Chen, B. Yang, S. Xu and X. Yan, *Energy Environ. Sci.*, 2019, **12**, 887–922; (*b*) X. Li, S. Yang, N. Feng, P. He and H. Zhou, *Chin. J. Catal.*, 2016, **37**, 1016–1024.
7 (*a*) L. Qie, Y. Lin, J. W. Connell, J. Xu and L. Dai, *Angew. Chem., Int. Ed.*, 2017, **56**, 6970–6974; (*b*) Z. Zhao, E. Wang, J. Wang, C. Liu and Z. Peng, *J. Mater. Chem. A*, 2021, **9**, 3290–3296.
8 (*a*) Z. Zhang, Q. Zhang, Y. Chen, J. Bao, X. Zhou, Z. Xie, J. Wei and Z. Zhou, *Angew. Chem., Int. Ed.*, 2015, **54**, 6550–6553; (*b*) Y. Jin, C. Hu, Q. Dai, Y. Xiao, Y. Lin, J. W. Connell, F. Chen and L. Dai, *Adv. Funct. Mater.*, 2018, **28**, 1804630; (*c*) X. Zhang, Q. Zhang, Z. Zhang, Y. Chen, Z. Xie, J. Wei and Z. Zhou, *Chem. Commun.*, 2015, **51**, 14636–14639; (*d*) C. Li, Z. Guo, B. Yang, Y. Liu, Y. Wang and Y. Xia, *Angew. Chem., Int. Ed.*, 2017, **56**, 9126–9130.
9 (*a*) B. Ge, Y. Sun, J. Guo, X. Yan, C. Fernandez and Q. Peng, *Small*, 2019, **15**, 1902220; (*b*) X. Zhang, C. Wang, H. Li, X.-G. Wang, Y.-N. Chen, Z. Xie and Z. Zhou, *J. Mater. Chem. A*, 2018, **6**, 2792–2796; (*c*) S. Li, Y. Liu, J. Zhou, S. Hong, Y. Dong, J. Wang, X. Gao, P. Qi, Y. Han and B. Wang, *Energy Environ. Sci.*, 2019, **12**, 1046–1054; (*d*) W. Ma, S. Lu, X. Lei, X. Liu and Y. Ding, *J. Mater. Chem. A*, 2018, **6**, 20829–20835.
10 (*a*) Y. Xing, Y. Yang, D. Li, M. Luo, N. Chen, Y. Ye, J. Qian, L. Li, D. Yang, F. Wu, R. Chen and S. Guo, *Adv. Mater.*, 2018, **30**, 1803124; (*b*) K. Li, Y. Li, Y. Wang, J. Ge, C. Liu and W. Xing, *Energy Environ. Sci.*, 2018, **11**, 1232–1239; (*c*) S. Yang, Y. Qiao, P. He, Y. Liu, Z. Cheng, J.-J. Zhu and H. Zhou, *Energy Environ. Sci.*, 2017, **10**, 972–978; (*d*) Y. Qiao, S. Xu, Y. Liu, J. Dai, H. Xie, Y. Yao, X. Mu, C. Chen, D. J. Kline, E. M. Hitz, B. Liu, J. Song, P. He, M. R. Zachariah and L. Hu, *Energy Environ. Sci.*, 2019, **12**, 1100–1107; (*e*) Y. Xing, K. Wang, N. Li, D. Su, W.-T. Wong, B. Huang and S. Guo, *Matter*, 2020, **2**, 1494–1508.
11 (*a*) S. Li, Y. Dong, J. Zhou, Y. Liu, J. Wang, X. Gao, Y. Han, P. Qi and B. Wang, *Energy Environ. Sci.*, 2018, **11**, 1318–1325; (*b*) Y. Zhang, R.-L. Zhong, M. Lu, J.-H. Wang, C. Jiang, G.-K. Gao, L.-Z. Dong, Y. Chen, S.-L. Li and Y.-Q. Lan, *ACS Cent. Sci.*, 2021, **7**, 175–182.
12 L. Liu, L. Zhang, K. Wang, H. Wu, H. Mao, L. Li, Z. Sun, S. Lu, D. Zhang, W. Yu and S. Ding, *ACS Appl. Mater. Interfaces*, 2020, **12**, 33846–33854.
13 (*a*) A. Mahmood, W. Guo, H. Tabassum and R. Zou, *Adv. Energy Mater.*, 2016, **6**, 1600423; (*b*) A. Khayum M, M. Ghosh, V. Vijayakumar, A. Halder, M. Nurhuda, S. Kumar, M. Addicoat, S. Kurungot and R. Banerjee, *Chem. Sci.*, 2019, **10**, 8889–8894.
14 K. Wang, X.-L. Lv, D. Feng, J. Li, S. Chen, J. Sun, L. Song, Y. Xie, J.-R. Li and H.-C. Zhou, *J. Am. Chem. Soc.*, 2016, **138**, 914–919.
15 A. Spek, *Acta Crystallogr., Sect. C: Cryst. Struct. Commun.*, 2015, **71**, 9–18.
16 A. Ahmadiparidari, R. E. Warburton, L. Majidi, M. Asadi, A. Chamaani, J. R. Jokisaari, S. Rastegar, Z. Hemmat, B. Sayahpour, R. S. Assary, B. Narayanan, P. Abbasi, P. C. Redfern, A. Ngo, M. Vörös, J. Greeley, R. Klie, L. A. Curtiss and A. Salehi-Khojin, *Adv. Mater.*, 2019, **31**, 1902518.

